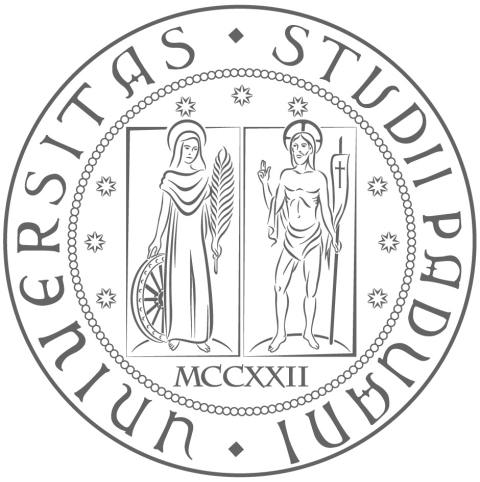

Università degli Studi di Padova

Dipartimento di Fisica e Astronomia
"Galileo Galilei"

Laurea Triennale in Fisica

The Cosmic Microwave Background Polarization

Candidato:
Davide Gurnari

Relatore:
Dott. Michele Liguori

Anno accademico 2016–2017

Contents

Introduction

The discover in 1965 that the Earth is bathed in all directions by an extremely uniform radiation with a black-body-like spectrum with the temperature of $2.7K$ constitutes one of the biggest advances in the last century Cosmology, providing one of the most convincing proofs for the Big Bang cosmological model. In 1992 the COBE satellite showed temperature fluctuations in the Cosmic Microwave Background radiation at the level of 1 part in 10^5. Furthermore, in 2002, the DASI experiment revealed a degree of linear polarization of the CMB photons. Over the last decades satisfying theoretical explanations for these anisotropies have been provided and the data analysis has led to the constrain of many cosmological parameters. Besides, the CMB polarization is considered to be one of the main actors in the quest for an experimental proof of one of the biggest open problems in modern Cosmology, the theory of inflation.

The CMB polarization is a complex subject and a formal description of all his aspect request mathematical techniques that vary from differential geometry to statistical mechanics. For this reason, especially in the last Chapter, we will sometimes avoid a mathematically exhaustive treatment in favour of a qualitative description that, in our hope, still manages to deliver a good understanding of the physics behind this phenomena.

Our work is organized in the following order: in Chapter 1 we will present some fundamental concept in modern Cosmology and in Chapter 2 we will introduce the statistical formalism that we will need for description of the CMB anisotropies. A description of the CMB, its relationship with the thermal history of the Universe and its most important properties will be given in Chapter 3, along with a dissertation about the temperature anisotropies and a qualitative explanation of the origin of these fluctuations. Chapter 4 will be devoted to Thomson scattering, how it can lead to a linear polarization pattern under certain conditions and the development of a mathematical formalism to describe a general polarization state. Finally, in Chapter 5 we will focus on the polarization of the CMB, we will build intuition about the possible causes of various polarization patterns generated by a single electron and the differences between them. Another formalism will be introduced in order to describe the polarization without the need of a specific reference frame and it will be used to explain the modulation of the polar-

ization modes over the last scattering surface. We will then understand how the detection of a B-mode in the CMB can be interpreted as the footprint of a primordial gravitational wave and so a strong proof of the theory of inflation.

Chapter 1

Cosmology

1.1 Cosmological Principle

The fundamental idea behind modern cosmology is the assertion that the place which we occupy in the Universe is not special in any way, a concept known as the cosmological principle. This leads to the belief that, on sufficiently large scales, the Universe is both homogeneous and isotropic. Homogeneity is the property of being identical everywhere in the space, while isotropy is the property of looking the same in every direction. Only in the last few decades technology advancements have led to convincing observational proofs that the Universe appears to be smooth on scales of hundreds of megaparsecs and more.

It is important though to stress the limits of this principle, the Universe is clearly not exactly homogeneous; homogeneity has to be defined in an average sense. As a matter of fact tiny variations from the average smoothness will be the key focus of this thesis.

1.2 Expansion of the Universe

The radial velocity of a celestial object can be measured thanks to the Doppler effect, for a receding luminal source the observed radiation will be redshifted by a factor

$$z = \frac{\lambda_r - \lambda_e}{\lambda_e}\,, \tag{1.1}$$

where λ_e and λ_r are respectively the emitted and the observed wavelength. It is an observational evidence that almost everything in the Universe appears to be moving away from us, and the recession grows linearly with the distance between the object and the observer. The discovery of this phenomenon is due to Edwin Hubble and is this described mathematically by the

$$\vec{v} = H_0 \vec{r}\,, \tag{1.2}$$

where H_0 is known as Hubble's constant. This led cosmologists to believe that our Universe is not static at all, but indeed it is currently expanding.

It is crucial to note that in an expanding Universe every observer sees all objects moving away, Hubble's law is not in contrast with the cosmological principle.

1.3 Friedmann Equations

1.3.1 First Friedmann Equation

Using only the cosmological principle and Newtonian gravity we can derive an equation that describes the expansion of the Universe.

First of all we consider an observer in an uniform expanding medium with mass density ρ and a particle of mass m at a distance r. The particle feels a force

$$F = \frac{GMm}{r^2} = \frac{4\pi G\rho r m}{3}\,; \tag{1.3}$$

the total energy of the particle will be

$$U = T + V = \frac{1}{2}m\dot{r}^2 - \frac{4\pi}{3}G\rho r^2 m\,, \tag{1.4}$$

where T in the kinetic energy and V the potential energy. Clearly U is conserved because the system is isolated.

Now we move to a different coordinate system, the comoving coordinates $\vec{x}$. These new coordinates are carried along with the expansion so objects remains at fixed location in the $\vec{x}$ system (in other words $\dot{x} = 0$). The relationship between the comoving coordinates and the $\vec{r}$, also known as physical coordinates, is

$$\vec{r} = a(t)\vec{x} \tag{1.5}$$

and the homogeneity property ensures that $a(t)$ is a function of time alone. The quantity $a(t)$ is the scale factor of the Universe and it is a measure of the expansion rate.

So we can rewrite the total energy of the particle

$$U = \frac{1}{2}m\dot{a}^2x^2 - \frac{4\pi}{3}G\rho a^2 r^2 m\,. \tag{1.6}$$

Multiplying both sides by $2/ma^2x^2$ and rearranging we obtain the Friedman equation

$$\left(\frac{\dot{a}}{a}\right)^2 = \frac{8\pi G}{3}\rho - \frac{kc^2}{a^2}\,, \tag{1.7}$$

where $kc^2 = -2U/mc^2x^2$

Since all the others terms in (1.7) are independent of x, in order to maintain homogeneity k must be x independent too. Furthermore both U

and x are time independent (the total energy is conserved and the comoving separation is fixed) so k must be a constant. Every expanding Universe has a fixed value of k, called curvature, and his signature defines the geometry of the Universe that can be flat, spherical or hyperbolic corresponding to $K = 0, > 0, < 0$ respectively.

1.3.2 Fluid Equation

In addition to the Friedmann equation (1.7) we need to account for the evolution of the density ρ, related to the pressure p of the material. We start by considering the first law of thermodynamics

$$dE + pdV = TdS \tag{1.8}$$

applied to an expanding volume V of unit comoving radius (so that the physical radius is a). From $E = mc^2$ we obtain

$$E = \frac{4\pi}{3} a^3 \rho c^2 \tag{1.9}$$

and so, deriving in dt

$$\frac{dE}{dt} = 4\pi a^2 \rho c^2 \frac{da}{dt} + \frac{4\pi}{3} a^3 \frac{d\rho}{dt} c^2 \,, \tag{1.10}$$

while for the volume

$$\frac{dV}{dt} = 4\pi a^2 \frac{da}{dt} \,. \tag{1.11}$$

Assuming a reversible expansion $dS = 0$ and substituting these into (1.8) gives

$$\dot{\rho} + 3\frac{\dot{a}}{a}\left(\rho + \frac{p}{c^2}\right) = 0 \tag{1.12}$$

1.3.3 Equation of State

In order to solve this equations a relationship between the density and the pressure is needed, know as the equation of state. The most general function can be written as $p = p(\rho)$, once it is specified the evolution of the Universe is determined by (1.7) and (1.12).

Usually in cosmology, to obtain such a relationship, two opposite limits are considered for the particles in the Universe:

- Matter: any type of material which exerts negligible pressure, also known as "non-relativistic matter". In this approximation $p = 0$ and the only non negligible interaction is the gravitational one;
- Radiation: particles moving at highly-relativistic speeds, their kinetic energy has to be taken into account. For example, the radiation pressure of the photons is $p = \rho c^2/3$.

A more general solution can be obtained with mixtures of these two, using a $\rho = \rho_{mat} + \rho_{rad}$.

1.3.4 Acceleration Equation

Using the Friedmann and the fluid equations we can obtain a formula for the acceleration of the scale factor. Differentiating (1.7) with respect to time we obtain

$$2\frac{\dot{a}}{a}\frac{a\ddot{a}-\dot{a}^2}{a^2} = \frac{8\pi G}{3}\dot{\rho} + 2\frac{kc^2\dot{a}}{a^3} \tag{1.13}$$

then we explicit $\dot{\rho}$ from (1.12)

$$\frac{\ddot{a}}{a} - \left(\frac{\dot{a}}{a}\right)^2 = -4\pi G\left(\rho + \frac{p}{c^2}\right) + \frac{kc^2}{a^2} \tag{1.14}$$

where we have simplified the factor $2\dot{a}/a$. Using again the (1.7) we have the acceleration equation

$$\frac{\ddot{a}}{a} = -\frac{4\pi G}{3}\left(\rho + \frac{3p}{c^2}\right). \tag{1.15}$$

From this equation it is easy to understand why the fact that the matter has a non zero pressure helps decelerate the expansion because the gravitational force is increased. It should also be noted that this new equation, which of course is not independent of (1.7) and (1.12), does not feature the constant k.

1.4 Hubble's Law Revisited

Given the velocity $\vec{v} = d\vec{r}/dt$ and remembering the (1.2), we can immediately write

$$\vec{v} = \frac{|\dot{\vec{r}}|}{|\vec{r}|}\vec{r} = \frac{\dot{a}}{a}\vec{r}. \tag{1.16}$$

So the parameter in the Hubble's law is

$$H(t) = \frac{\dot{a}}{a} \tag{1.17}$$

and it is important to notice that it is not a constant because of its time dipendency and his evolution is given by the Friedmann equation.

1.5 Hints of General Relativistic Cosmology

The natural playground for the study of cosmology is General Relativity, in order to obtain the Friedmann's equations in the most rigorous way one should have started considering the Einstein's field equations and not their approximation, Newton's theory of gravity. But this formal approach goes beyond the aim of this thesis; moreover, it could be shown that the Friedmann's equations calculated using General Relativity are exactly the same that we obtained using the Newtonian limit in our euristic derivation.

Nevertheless we will now use this formalism to obtain a relation between the redshift and the scale factor.

1.5.1 Redshift and scale factor

The most general solution of Einstein's equations for an homogeneous, isotropic expanding Universe is given by the Robertson-Walker metric

$$ds^2 = -c^2dt^2 + a(t)\left[\frac{dr^2}{1-kr^2} + r^2(d\theta^2 + \sin^2\theta d\phi^2)\right] \tag{1.18}$$

where spherical comoving coordinates are being used and $a(t)$ is the scale factor.

A key concept in both special and general relativity is that a light ray obeys

$$ds^2 = 0\,. \tag{1.19}$$

Considering a radial ray, which means that $d\theta = d\phi = 0$, this equation gives in the R-W metric

$$\frac{c\ dt}{a(t)} = \frac{dr}{\sqrt{1-kr^2}}\,. \tag{1.20}$$

In order to find the time it takes to get from $r = 0$ to $r = r_0$ we simply integrate

$$\int_{t_e}^{t_r} \frac{c\ dt}{a(t)} = \int_0^{r_0} \frac{dr}{\sqrt{1-kr^2}} \tag{1.21}$$

where "e" stands for emission and "r" reception.

If we consider another light ray emitted after a short time interval dt_e and thus received a dt_r after the first ray reception

$$\int_{t_e+dt_e}^{t_r+dt_r} \frac{c\ dt}{a(t)} = \int_0^{r_0} \frac{dr}{\sqrt{1-kr^2}}\,, \tag{1.22}$$

because in the limit $dt_{e,r} \to 0$ all objects are still at the same coordinates. So we can write

$$\int_{t_e}^{t_r} \frac{c\ dt}{a(t)} = \int_{t_e+dt_e}^{t_r+dt_r} \frac{c\ dt}{a(t)} \tag{1.23}$$

and rearranging

$$\int_{t_e}^{t_e+dt_e} \frac{c\ dt}{a(t)} = \int_{t_r}^{t_r+dt_r} \frac{c\ dt}{a(t)}\,. \tag{1.24}$$

In the limit $dt_{e,r} \to 0$ we finally obtain

$$\frac{dt_r}{a(t_r)} = \frac{dt_e}{a(t_e)}\,. \tag{1.25}$$

If the Universe is expanding then $a(t_r) > a(t_e)$, that gives $dt_r > dt_e$, which means that the time interval between the two rays increases as the Universe expands.

Now, if we consider the two rays being on consecutive crests of a single wave and keeping in mind that $\lambda \propto dt \propto a(t)$, we can thus write

$$\frac{\lambda_r}{\lambda_e} = \frac{a(t_r)}{a(t_e)} \,. \tag{1.26}$$

Confronting this result with the (1.1) we can relate the redshift to the scale factor

$$\frac{a(t_r)}{a(t_e)} \equiv 1 + z \,. \tag{1.27}$$

In cosmology is quite common to use the term "redshift" to describe both distances from objects and epochs in the life of the Universe. For example, saying that an object is at redshift z means that it is at a distance such that its light has redshifted by a factor $(1 + z)$ in the time it has taken to reach us. When referring to the Universe, a redshift of z means the time when the Universe was $1/(1 + z)$ of its present size.

Chapter 2

Perturbations

In this chapter we will introduce some statistical tools that are going to be widely used in the discussion of CMB anisotropies. The key idea is that a generic perturbation can be represented as a superposition of plane waves which, while they are evolving linearly, evolve independently of each other. Thus we will describe linear perturbations in terms of their spectral composition and analyze their spectral properties.

2.1 Density Perturbations

In this section we will focus on a perturbation in the density of matter in the Universe.

We can start by considering a volume V_u, for example a cube of side L. V_u can be said to be a 'fair sample' of the Universe if $L \gg l_s$, where l_s is the maximum scale at which there is significant structure due to perturbations. If we denote with $\langle\rho\rangle$ the mean density in V_u and with $\rho(\vec{x})$ the density in a specific point, we can define the fluctuation as

$$\delta(\vec{x}) = \frac{\rho(\vec{x}) - \langle\rho\rangle}{\langle\rho\rangle} \,. \tag{2.1}$$

We then express this as a Fourier series

$$\delta(\vec{x}) = \sum_{\vec{k}} \delta_{\vec{k}} \exp\left(i\vec{k}\cdot\vec{x}\right) = \sum_{\vec{k}} \delta^*_{\vec{k}} \exp\left(-i\vec{k}\cdot\vec{x}\right) . \tag{2.2}$$

Assuming periodic boundary conditions $\delta(L, y, z) = \delta(0, y, z)$ et simila requires that the components of the wavevector $\vec{k}$ must be

$$k_i = n_i \frac{2\pi}{L} \,. \tag{2.3}$$

with $i = 1, 2, 3$ and n_i integer.

The coefficients $\delta_{\vec{k}}$ are complex quantities given by

$$\delta_{\vec{k}} = \frac{1}{V_u} \int_{V_u} \delta_{\vec{x}} \exp\left(-i\vec{k} \cdot \vec{x}\right) d\vec{x} \tag{2.4}$$

with two additional conditions: conservation of mass in V_u gives $\delta_{\vec{k}=0} = 0$ and reality of $\delta_{\vec{x}}$ gives $\delta^*_{\vec{k}} = \delta_{-\vec{k}}$.

2.2 Power Spectrum

Choosing a different volume V_u', the perturbation in this volume will be again represented by a series like (2.2) but the coefficients $\delta_{\vec{k}}$ will be different. If we consider a large number of these volumes the mean value of the fluctuation $\delta(\vec{x}) \equiv \delta$ across the ensemble will be identically zero by definition, but its mean square value, called its variance, will be not. One could indeed show that

$$\sigma^2 \equiv \langle \delta^2 \rangle = \sum_{\vec{k}} \langle |\delta_{\vec{k}}|^2 \rangle = \frac{1}{V_u} \sum_{\vec{k}} \delta^2_{\vec{k}} \,. \tag{2.5}$$

If we now take the limit $V_u \to \infty$ assuming that there is no dependence on the direction of $\vec{k}$ but only on $k = |\vec{k}|$ (this means that the density field is statistically homogeneous and isotropic, according to the cosmological principle)

$$\sigma^2 = \frac{1}{V_u} \sum_{\vec{k}} \delta^2_{\vec{k}} \to \frac{1}{2\pi^2} \int_0^\infty P(k) k^2 dk \tag{2.6}$$

where we defined $\delta^2_k = P(k)$. This quantity is called the power spectrum and describes the amplitude of fluctuations on different length scales. Usually one assumes that the power spectrum is given by a power law $P(k) = Ak^n$ and the exponent n is called the spectral index.

We can also write equation (4.10) in the form

$$\sigma^2 = \frac{1}{2\pi^2} \int_0^\infty P(k) k^2 dk = \int_0^\infty \Delta(k) d\ln(k) \,, \tag{2.7}$$

where the dimensional quantity

$$\Delta(k) = \frac{1}{2\pi^2} P(k) k^3$$

represents the contribution to the variance per unit logarithmic interval in k.

Chapter 3

The Cosmic Microwave Background Radiation

In 1965 Penzias and Wilson accidentally discovered that the Earth is bathed in all directions by a radiation whose spectrum is extremely close to the one generated by a black-body with temperature

$$T_0 = 2.725 \pm 0.001K \ . \tag{3.1}$$

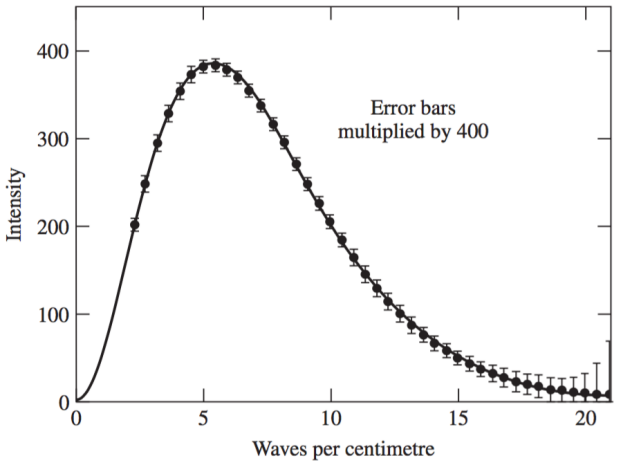

Figure 3.1: Data measured by the FIRAS experiment on the COBE satellite show a perfect fit with a black-body curve. The error bars had to be multiplied by 400 to make them visible on this plot.

This discovery had a huge impact on modern cosmology, it definitely ruled out the Steady State Universe hypothesis in favour of the Hot Big Bang hypothesis to explain the origin of the Universe. Furthermore the uniformity of the radiation is the best evidence of the cosmological principle for large scales.

3.1 Origin of the CMB

3.1.1 Decoupling

According to the Hot Big Bang theory, the Universe started hot and dense and then expanded and cooled. In the early Universe the typical energy of a photon in the thermal distribution was a lot higher than the $13.6eV$ needed to ionize hydrogen atoms, so it was not possible for atoms to exists at that epoch. The Universe was therefore a ionized plasma of electrons and nuclei (also called a photon-baryon fluid), in which electrons can be considered free. Because photons interact strongly with free electrons via Thompson scattering [1], the mean free path of any electron was thus very short; we could say that photons were tightly glued to matter and the Universe was opaque to radiation. As the Universe expanded and cooled down, the photons lost more and more energy due to redshift. When the Universe was about $300'000$ years old the temperature dropped below $3000K$ allowing atomic hydrogen to form in a process known as recombination. Because the interaction between photons and electrons in a atom (also know as Rayleigh scattering) is much weaker, photons where then able to travel uninterrupted and finally reach us. Cosmologist use to say that the Universe switched from being opaque to being transparent and this epoch is known as decoupling.

3.1.2 Last Scattering Surface

The photons observed in the CMB come from a distance close to the size of the observable Universe; because of this we see them originated on the surface of a very large sphere centred in our position, called the surface of last scattering. As we said when talking about Hubble's law in Chapter 1, there is nothing special about our position, photons originated in every point of the Universe and every possible observer will see them coming from a sphere centred in his location.

3.1.3 Redshift of CMB photons

It is a well known result that for a black-body at temperature T the energy density in a frequency interval $d\nu$ is

$$\epsilon(\nu)\, d\nu = \frac{8\pi h}{c^3} \frac{\nu^3\, d\nu}{\exp(h\nu/k_B T) - 1}\,, \tag{3.2}$$

where h and k_B are respectively the Plank and the Boltzmann constant.

The total energy density can be obtained setting $y = h\nu/k_B T$ and then integrating

$$\epsilon_{rad} = \frac{8\pi k_B^4}{h^3 c^3} T^4 \int_0^\infty \frac{y^3\, dy}{e^y - 1} = \alpha T^4\,, \tag{3.3}$$

[1] For a mathematical explanation of this process see the next chapter

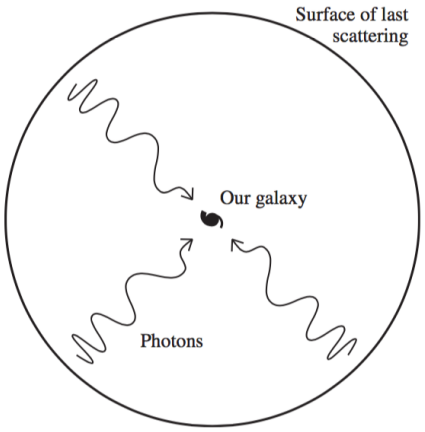

Figure 3.2: Schematic view of the last scattering sphere

where the constant is

$$\alpha = \frac{\pi^2 k_B^4}{15\hbar c^3} \,. \tag{3.4}$$

The energy density is related to the mass density via the

$$\epsilon_{rad} \equiv \rho_{rad} c^2 \,, \tag{3.5}$$

but for a radiation dominated Universe the Friedmann equations tell us that the density radiation evolves with the expansion

$$\rho_{rad} \propto \frac{1}{a^4} \,, \tag{3.6}$$

where a is the scale factor.

Combining with the (3.3) we obtain

$$T \propto \frac{1}{a} \,. \tag{3.7}$$

This means that the Universe cools down as it expands, the frequency ν is redshifted in proportion to $1/a$ but the black-body form is preserved in a lower temperature

$$T_{final} = T_{initial} \frac{a_{initial}}{a_{final}} \,. \tag{3.8}$$

This property can be understood by looking carefully at equation (3.3): firstly, the exponential is a function of ν/T so it is a-independent. Secondly, the ν^3 on the numerator scales as the inverse volume, exactly like the energy density on the left-hand side.

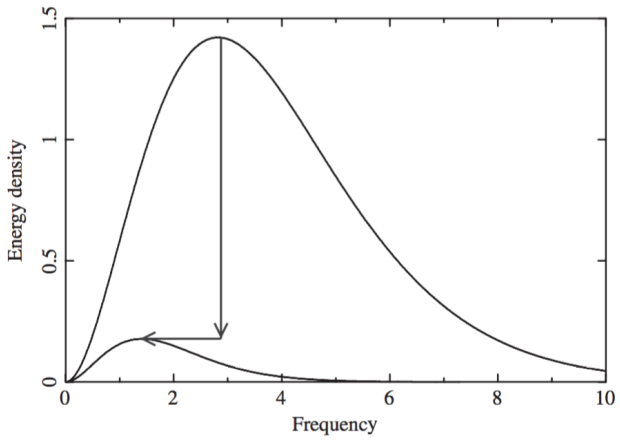

Figure 3.3: Evolution of the black-body spectrum during the expansion of the Universe.

3.2 CMB Temperature Anisotropies

We said that the CMB was found to be remarkably uniform across the sky. As a matter of fact, it was not until 1992 that the COBE satellite discovered temperature variations at the level of 1 part in 10^5. In analogy with the density fluctuations described in Chapter 2, we can define a temperature fluctuation function of the position in the sky $\hat{n} = (\theta, \phi)$

$$\Theta(\hat{n}) = \frac{\Delta T}{T}(\theta, \phi) = \frac{T(\theta, \phi) - \bar{T}}{\bar{T}} \, . \tag{3.9}$$

We now want to carry out an expansion like we did in (2.2) but this time we must use spherical harmonics $Y_{lm}(\theta, \phi)$ because we are operating on the surface of a sphere

$$\Theta(\hat{n}) = \sum_{l=1}^{\infty} \sum_{m=-l}^{l} \Theta_{lm} Y_{lm}(\hat{n}) \, , \tag{3.10}$$

where the multipole moments of the temperature field are

$$\Theta_{lm} = \int d\hat{n} Y_l m^*(\hat{n}) \Theta(\hat{n}) \tag{3.11}$$

and, if the fluctuations are Gaussian, they are fully charaterized by their radiation angular power spectrum C_l defined by

$$\langle \Theta^*_{lm} \Theta_{l'm'} \rangle = \delta_{ll'} \delta_{mm'} C_l \, . \tag{3.12}$$

Note that the C_l cannot depend on the m index because of the rotational invariance of the statistical properties.

From a theoretical point of view, the (3.12) could be thought as an average over all the possible observers in our Universe (every observer sees his last scattering surface). But all the possible experiments can only study the CMB as seen from Earth so all they can do is average over the possible values of index m. The difference between our region of the Universe as compared to the average is known as cosmic variance. This sets a limit to the accuracy of power spectra measurements, there are only $2l+1$ m-samples of each multipole moment, and leads to an inevitable error of

$$\Delta C_l = \sqrt{\frac{2}{2l+1}} C_l \,. \tag{3.13}$$

On small sections of the sky, the spherical harmonic analysis becomes ordinary Fourier analysis in two dimensions, in this limit the variance of the field is $\int d^2l C_l/(2\pi)^2$ and the power spectrum is conventionally displayed as

$$\Delta_T^2 \equiv \frac{l(l+1)}{2\pi} C_l T^2 \tag{3.14}$$

the power per logarithmic interval in wavenumber for $\mathrm{l} \ll 1$.

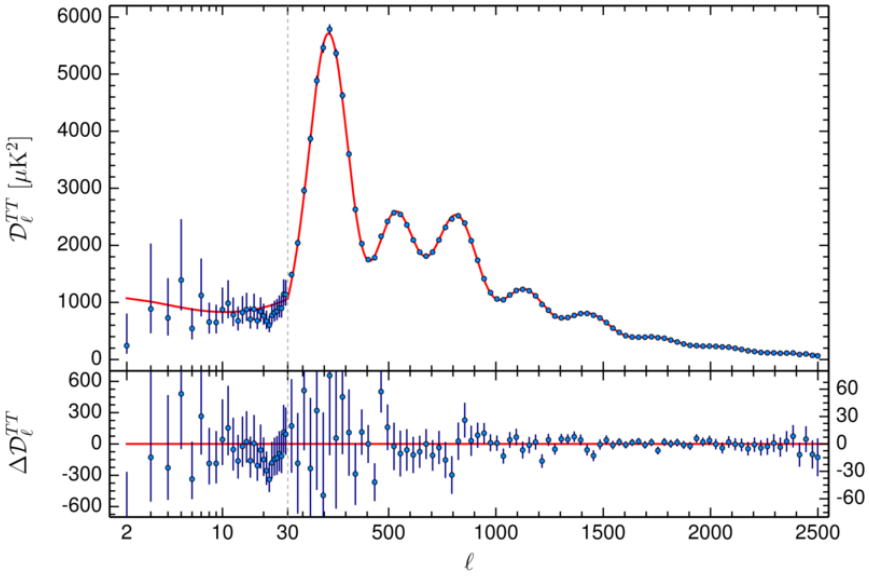

Figure 3.4: Planck 2015 TT power spectrum. The $\hat{x}$-axis is logarithmic up to $l = 30$ and linear at higher l. The red line is the Planck best-fit primordial power spectrum. Residuals with respect to this model are shown in the lower panel. The error bars show $\pm 1\sigma$ uncertainties.

3.2.1 About the Dipole

The most prominent feature in the CMB is the $l = 1$ perturbation, known as the dipole. But this pattern is generated simply because the Earth is

moving with respect to the CMB and so the observed temperature appears redshifted or blueshifted because of the Doppler effect. As a matter of fact calculations that take into account the Sun's revolution around the galaxy explains very well the dipole data. For this reason $l = 2$ is the smallest value considered when studying the intrinsic properties of the background. Maps of the CMB are always shown with the dipole already removed.

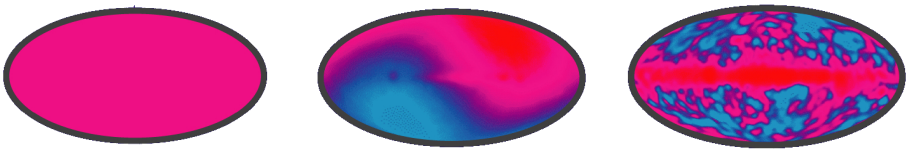

(a) (b) (c)

Figure 3.5: Temperature maps of the CMB: no variations whatsoever at the level of 1 part in 1000 (a), if we turn up the contrast a dipole pattern appears (b), when the dipole is removed anisotropies emerges (c). The line around the equator is a contamination from our own galaxy.

3.3 Origin of the Fluctuations

3.3.1 Inflation and Acoustic Oscillations

The theory of inflation was introduced in the '80s by various authors in order to solve some critical issues in the Standard Cosmological Model such as the horizon problem and the flatness problem. According to this theory the early Universe went through a phase of exponential expansion that ended 10^{-34} seconds after the Big Bang that can be described as the action of a scalar field Φ generating a negative pressure.

An exhaustive presentation of inflationary theories is not the aim of this thesis but there is a key point that needs to be stressed. In this period of rapid expansion random quantum fluctuations were stretched into cosmic scales, creating fluctuations in the energy density. But these variations imply anisotropies in the local gravitational potential, regions of high density generate potential wells while regions of low density generate potential hills.

As we said in the previous sections, before recombination the matter in the Universe can be described as a photon-baryon fluid. In the potential wells gravity tends to compress the fluid but its radiation pressure opposes to it, this results in acoustic oscillations. Like a gas, the fluid will heat up when compressing while it will cool down when expanding. This leads to temperature anisotropies in the CMB that follow the oscillations. These oscillation modes can be linked to the peaks in the temperature power spectrum (see fig. 3.4), the first peak represents the mode that compressed once inside potential wells before recombination, the second the mode that com-

pressed and then rarefied, and so one. The measurement and analysis of these peaks leads to precise estimation of various cosmological parameters.

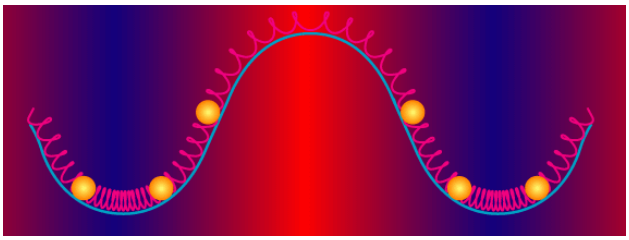

Figure 3.6: Potential wells and hills cause the fluid (here depicted as spings) to compress and expand, this leads to oscillations. Temperature fluctuations follow density variations. In this picture color blue means hot while red is cold.

Because inflation lays down potential fluctuations on all scales we can decompose the fluctuations into plane waves using the Fourier transform. According to the mathematics each mode behave independently and so we can think of each individually. From now on then we will focus on only one plane wave perturbation.

3.3.2 Inflation and Gravitational Waves

Another important prediction of any inflationary model is the production of primordial gravitational waves. The explosive expansion during inflation would have created ripples in the fabric of spacetime, perturbation that can be viewed as gravitational waves. The amplitude of these waves is predicted to be proportional to the expansion rate during inflation, which in turn is proportional to the inflation energy scale squared. In the last Chapter we will see that some patterns in the CMB polarization can be linked to these primordial gravitational waves, the future detection of these patterns would be an important proof in support of the theory of inflation.

3.3.3 From Spatial Inhomegeneity to Angular Anisotropy.

The fluid stop oscillating at recombination, the photons are no longer strictly coupled with the baryons and (after a little period of random walk because recombination does not occur instantaneously) they start streaming unimpeded.

Let consider a generic observer, right after recombination he will see an isotropic CMB but, as time passes, he will be reached by photons from more and more distant regions. With reference to the figure below, considering a single plane wave mode, the CMB pattern becomes a dipole, then a quadrupole and so on. After billions of years every observer in the Universe see a fine angular scale structure in the CMB temperature

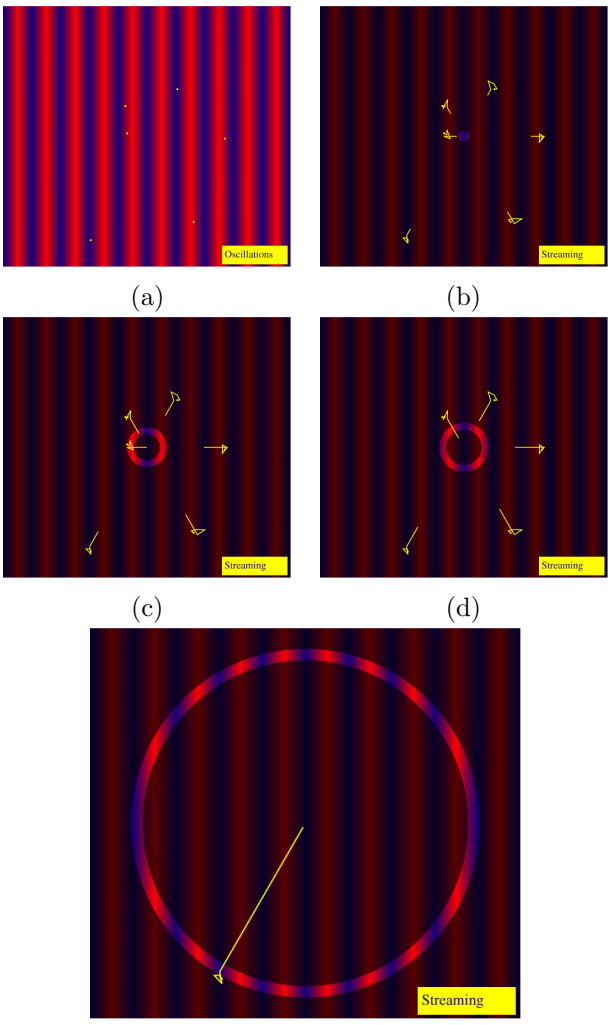

Figure 3.7: Oscillations before recombination (a). After recombination photons (yellow lines) start moving and reach the observer who will see the CMB pattern evolve from a monopole (b), to a dipole (c), quadrupole (d) and so on. Today we see a fine angular structure (e)

Chapter 4

Polarization

4.1 Thomson Scattering From a Single Wave

Thomson scattering is the scattering of electromagnetic radiation by a free electron. If an electromagnetic wave is incident on a free charged particle, the particle will be accelerated by the electric field and in response emit radiation. This process is the low energy limit of Compton scattering and can be described in a classical, non-relativistic way.

An useful tool to describe this phenomena is the differential cross section, defined as the radiated intensity per unit solid angle divided by the incoming intensity per unit area

$$\frac{d\sigma}{d\Omega} = \frac{1}{I_0}\frac{dW}{d\Omega} \tag{4.1}$$

where I_0 and W are respectively the incident energy flux and the emitted power.

4.1.1 Linearly Polarized Incident Wave

For an incident linearly polarized plane wave propagating in the $\hat{z}$ direction

$$\vec{E}_{in} = \vec{E}_0 \cos(\omega(t-z))\,; \qquad \vec{B}_{in} = \hat{z} \times \vec{E}_{in} \tag{4.2}$$

the incident flux is the time-averaged Poynting vector

$$I_0 = \langle|\vec{S}|\rangle = \langle|\vec{E}_0|^2\rangle = \langle|\vec{E}_0\cos(\omega(t-z))|^2\rangle = \frac{1}{2}E_0^2 \tag{4.3}$$

where we have denoted with $\langle\cdot\rangle$ the time average over a period.

In our hypothesis the velocity v of the electron (we will reintroduce units of c at the end of this section), when moved by the incident radiation, is $v \ll 1$. We can thus use the dipole approximation.

The force on the electron is, from the Lorentz formula

$$m\frac{d^2}{dt^2}\vec{y}(t) = e(\vec{E}_{in} + \vec{v} \times \vec{B}_i n)\,; \tag{4.4}$$

since in a plane wave $|\vec{E}_{in}| = |\vec{B}_{in}|$ and $v \ll 1$ we can neglect the magnetic field

$$m\frac{d^2}{dt^2}\vec{y}(t) = e\vec{E}_{in}(t, \vec{y}(t)) \simeq e\vec{E}_{in}(t, 0) = e\vec{E}_0 \cos(\omega t)\,. \tag{4.5}$$

The last approximation is valid because $\vec{E}, \vec{B} \perp \hat{z}$. The particle will then move in a direction orthogonal to $\hat{z}$ while the fields depend only on the z coordinate.

The equation of motion can be easily obtained from integration

$$\vec{y}(t) = -\frac{e}{m\omega^2}\vec{E}_0 \cos(\omega t)\,. \tag{4.6}$$

Besides, we can write the emitted radiation fields in terms of the dipole moment $\vec{D}(t) = e\vec{y}(t)$

$$\vec{E}(t, r) = -\frac{1}{4\pi r}\left[\ddot{\vec{D}} - \left(\vec{n}\cdot\ddot{\vec{D}}\right)\vec{n}\right] = -\frac{e}{4\pi m r}\left[\vec{E}_0 - \left(\vec{n}\cdot\vec{E}_0\right)\vec{n}\right]\cos(\omega(t-r)) \tag{4.7}$$

$$\vec{B}(t, r) = \vec{n}\times\vec{E}(t, r) \tag{4.8}$$

where $\vec{n}$ is the observation vector.

The average power per unit solid angle is

$$\left\langle\frac{dW}{d\Omega}\right\rangle = r^2\langle|\vec{E}|^2\rangle = \frac{1}{2}\frac{e^4}{16\pi^2 m^2}\left[|\vec{E}_0|^2 - \left(\vec{n}\cdot\vec{E}_0\right)^2\right] \tag{4.9}$$

If we name Θ the angle between $\vec{n}$ and $\vec{E}_0$ we have

$$\left\langle\frac{dW}{d\Omega}\right\rangle = \frac{e^4}{32\pi^2 m^2}|\vec{E}_0|^2 \sin^2\Theta \tag{4.10}$$

and the cross section becomes

$$\frac{d\sigma}{d\Omega} = r_0^2 \sin^2\Theta\,, \tag{4.11}$$

where r_0 is the classical electron radius defined as (reintroducing the c)

$$r_0 = \frac{e^2}{4\pi m c^2}\,. \tag{4.12}$$

From (4.7) we note that the scattered radiation is polarized in the plane of the incident polarization (the direction of the electric field) and the scattering direction $\vec{n}$.

4.1.2 Unpolarized Incident Wave

If the incident wave is unpolarized there will not be a preferred direction for E_0, every plane orthogonal to $\hat{z}$ is equiprobable. We will have to average (denoted as $\langle\langle\cdot\rangle\rangle$) over all the possible orientations

$$\langle\langle E_{0,x}\rangle\rangle = \langle\langle E_{0,y}\rangle\rangle = 0 \tag{4.13}$$

$$\langle\langle E_{0,x}^2\rangle\rangle = \langle\langle E_{0,y}^2\rangle\rangle = \frac{1}{2}|\vec{E}_0|^2 \tag{4.14}$$

$$\langle\langle E_{0,x}E_{0,y}\rangle\rangle = 0\,. \tag{4.15}$$

If $\vec{E}_0$ has no fixed direction, the angle Θ used in the previous section is not well defined. Let θ be the angle between $\hat{z}$ and the observation vector $\vec{n}$, we can write

$$\begin{aligned}\langle\langle(\vec{n}\cdot\vec{E}_0\rangle\rangle =& n_x^2\langle\langle E_{0,x}^2\rangle\rangle + n_y^2\langle\langle E_{0,y}^2\rangle\rangle + 2n_xn_y\langle\langle E_{0,x}E_{0,y}\rangle\rangle = \\ =& \frac{1}{2}|\vec{E}_0|^2(n_x^2+n_y^2) = \frac{1}{2}|\vec{E}_0|^2\sin^2\theta\end{aligned} \tag{4.16}$$

For an unpolarized incident wave equation (4.10) becomes

$$\left\langle\frac{dW}{d\Omega}\right\rangle_{np} = \frac{e^4}{32\pi^2m^2}|\vec{E}_0|^2(1-\frac{1}{2}\sin^2\theta) = \frac{e^4}{64\pi^2m^2}|\vec{E}_0|^2(1+\cos^2\theta) \tag{4.17}$$

and

$$\frac{d\sigma_{np}}{d\Omega} = r_0^2\frac{1+\cos^2\theta}{2}\,. \tag{4.18}$$

For a non polarized incident wave the polarization of the scattered radiation depends on θ. Along the incident direction $\theta = 0$ we see no net polarization since all directions in the plane are equivalent. On the other hand, if we look at $\theta = \pi/2$, perpendicular to the incident wave, we see complete linear polarization, because the electron's motion is confined to a plane normal to the incident radiation.

4.1.3 Total Thomson Cross Section

Integrating the (4.18) over the solid angle we obtain

$$\sigma_{Tnp} = \int\frac{d\sigma_{np}}{d\Omega}d\Omega = 2\pi\int_{-1}^{1}\frac{d\sigma_{np}}{d\Omega}d\cos\theta = 2\pi r_0^2\int_{-1}^{1}\frac{1+\cos^2\theta}{2}d\cos\theta = \frac{8\pi}{3}r_0^2\,. \tag{4.19}$$

The same result can be obtained integrating the cross section for a polarized incident wave (4.11)

$$\sigma_T = \int\frac{d\sigma}{d\Omega}d\Omega = 2\pi r_0^2\int_{-1}^{1}(1-\cos^2\Theta)d\cos\Theta = \frac{8\pi}{3}r_0^2\,, \tag{4.20}$$

but one must be careful defining different polar coordinates for the two angles.

An intuitive explanation for this equality is that at rest has no net direction intrinsically defined.

We can express the cross section in another way, with focus on the polarization

$$\frac{d\sigma}{d\Omega} = \frac{3\sigma_T}{8\pi}|\hat{\epsilon}' \cdot \hat{\epsilon}| \tag{4.21}$$

where $\hat{\epsilon}'$ and $\hat{\epsilon}$ are the directions of incoming and outgoing polarization, respectively.

4.2 Polarization From Thomson Scattering

Starting from this section we are going to consider not a single incident wave but an incoming radiation field.

Thomson scattering produces polarization only when the incident field has a quadrupole moment. The reason why this happen can be intuitively understood. With references to the following pictures, we consider incoming radiation from the left being scattered by 90 degrees out of the screen. Since light cannot be polarized along its direction of motion, only one linear polarization state gets scattered (a).

But there is nothing particularly special about light coming in from the left, if we consider also light coming in from the top the outgoing radiation will possesse both polarization states. If the incoming radiation from the left and top are of equal intensity, the result is no polarization in the outgoing direction (b).

Only if the intensity of the radiation varies at 90 degrees, in other words the distribution has a quadrupole pattern, does a net linear polarization result (c).

In the next sections we will show how such a behaviour can be described mathematically, but first we need to introduce some parameters to quantitatively describe polarization.

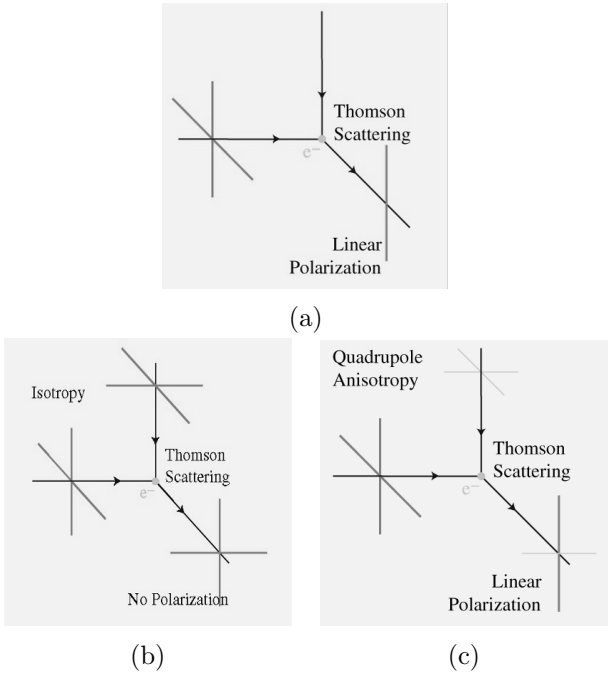

Figure 4.1: Thomson scattering on a single electron, only a quadrupole anisotropy in the incident field produced net linear polarization scattered

4.3 Stokes Parameters

A monochromatic electromagnetic wave propagating in the $\hat{z}$ direction has an electric field whose components are

$$E_x = a_x \cos(\omega t + \epsilon_x)\,; \qquad E_y = a_y \cos(\omega t + \epsilon_y)\,. \tag{4.22}$$

We can then define the Stokes parameters in a plane orthogonal to the direction of propagation as following

$$I = a_x^2 + a_y^2 \tag{4.23}$$
$$Q = a_x^2 - a_y^2 \tag{4.24}$$
$$U = 2a_x a_y \cos(\epsilon_x - \epsilon_y) \tag{4.25}$$
$$V = 2a_x a_y \sin(\epsilon_x - \epsilon_y) \tag{4.26}$$

where I is the intensity of the wave, Q and U are the linear-polarization parameters and V is the circular-polarization parameter. Thomson scattering induces no circular polarization, so V will not play a role in our analysis. Q represents the polarization in the $x - y$ direction while U represents its component along axes rotated by 45°.

Figure 4.2: Various combinations of Q and U describe different linear polarization states.

4.3.1 Behaviour under rotations

If we consider a rotation of the $x-y$ axes by an angle α the new coordinates will be

$$\begin{pmatrix} x' \\ y' \end{pmatrix} = \begin{pmatrix} \cos\alpha & \sin\alpha \\ -\sin\alpha & \cos\alpha \end{pmatrix} \begin{pmatrix} x \\ y \end{pmatrix} . \tag{4.27}$$

But the Stokes parameters (Q, U) will transform as

$$\begin{pmatrix} Q' \\ U' \end{pmatrix} = \begin{pmatrix} \cos 2\alpha & \sin 2\alpha \\ -\sin 2\alpha & \cos 2\alpha \end{pmatrix} \begin{pmatrix} Q \\ U \end{pmatrix} . \tag{4.28}$$

So (Q, U) behave like the components of a symmetric trace-free 2×2 tensor P_{ij} that, under a generical coordinate transformation

$$x'_i = A^k_i x_k \, , \tag{4.29}$$

transforms as

$$P'_{ij} = A^k_i A^l_j P_{kl} \, . \tag{4.30}$$

More explicitly

$$\begin{pmatrix} Q' & U' \\ U' & -Q' \end{pmatrix} = \begin{pmatrix} \cos\alpha & \sin\alpha \\ -\sin\alpha & \cos\alpha \end{pmatrix} \begin{pmatrix} Q & U \\ U & -Q \end{pmatrix} \begin{pmatrix} \cos\alpha & -\sin\alpha \\ \sin\alpha & \cos\alpha \end{pmatrix} . \tag{4.31}$$

We can define the polarization amplitute $|P|^2 = \sqrt{Q^2 + P^2}$ and his orientation to the $\hat{x}$ axes $\alpha = \frac{1}{2}\arctan(U/Q)$. Note that it is an headless vector, it transforms into itself for a π rotation, it behaves like a spin-2 object (or a 2×2 vector). We can also write the polarization as a complex number

$$P = |P| e^{2i\alpha} = Q + iU \, . \tag{4.32}$$

4.4 Polarization and Quadrupoles

In this section we will show that, if we consider a radiation field with intensity $I(\hat{n}') = \sum a_{lm} Y_{lm}(\hat{n}')$ incident on an electron e^-, the radiation scattered in the $\hat{z}$ direction will be linearly polarized only if the incident radiation has a quadrupole moment.

We will denote the incoming polarization vectors with $\hat{\epsilon}_i'$ and the outgoing with $\hat{\epsilon}_i$. Because we are considering outgoing photons in the $\hat{z}$ direction we can chose the outgoing polarization axes as $\hat{\epsilon}_1 = \hat{x}$ and $\hat{\epsilon}_2 = \hat{y}$. For an incoming photon from a general direction $\hat{n}'$ we will take the incoming polarization vectors to be $\hat{\epsilon}_1' = \hat{\theta}'$ and $\hat{\epsilon}_2' = \hat{\phi}'$ the standard unit vectors perpendicular to the position vector. In Cartesian coordinates this three vectors are:

$$\hat{n}'(\theta', \phi') = (\sin\theta' \cos\phi', \sin\theta' \sin\phi', \cos\theta') \tag{4.33}$$

$$\hat{\epsilon}_1'(\theta', \phi') = (\cos\theta' \cos\phi', \cos\theta' \sin\phi', -\sin\theta') \tag{4.34}$$

$$\hat{\epsilon}_2'(\theta', \phi') = (-\sin\phi', \cos\phi', 0) \tag{4.35}$$

where ϕ is the azimuthal angle. It is easy to verify that these three vectors are orthonormal.

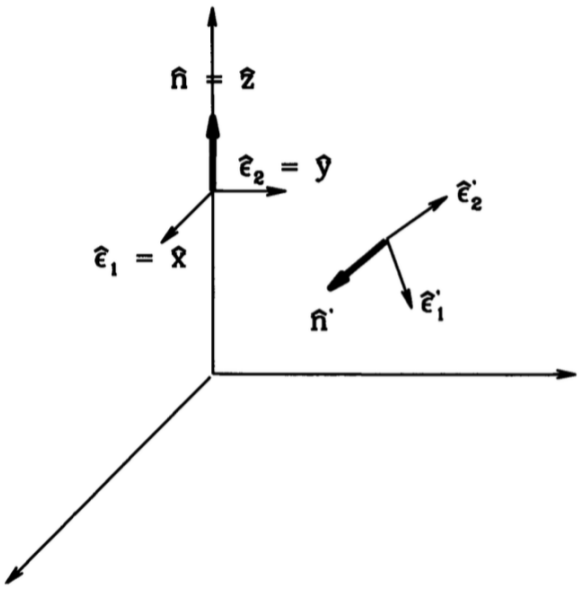

Figure 4.3: Incoming photon in the $\hat{n}'$ direction. Scattering produces an outgoing photon in the $\hat{n} = \hat{z}$ direction.

The cross-section for outgoing photons polarized in the $\hat{e}_i$ direction is

proportional to

$$\sum_{j=1}^{2}|\hat{e}_i(\hat{n})\cdot\hat{e}'_j(\hat{n}')|^2 \tag{4.36}$$

The Q polarization is the difference between the cross section for $i=1$ and $i=2$

$$\sum_{j=1}^{2}|\hat{e}_1(\hat{n})\cdot\hat{e}'_j(\hat{n}')|^2-\sum_{j=1}^{2}|\hat{e}_2(\hat{n})\cdot\hat{e}'_j(\hat{n}')|^2=\sum_{j=1}^{2}\left(|\hat{x}\cdot\hat{e}'_j(\hat{n}')|^2-|\hat{y}\cdot\hat{e}'_j(\hat{n}')|^2\right). \tag{4.37}$$

Integrating over all incoming directions $\hat{n}'$ we obtain

$$Q(\hat{z})=A\int d\Omega'\,I(\hat{n}')\sum_{j=1}^{2}\left(|\hat{x}\cdot\hat{e}'_j(\hat{n}')|^2-|\hat{y}\cdot\hat{e}'_j(\hat{n}')|^2\right). \tag{4.38}$$

where A is a normalization constant. Note that I depends only on $\hat{n}'$, not on the $\hat{e}'_j$, we have assumed that the incoming radiation is unpolarized.

If we express $\hat{e}'_1$ and $\hat{e}'_2$ in Cartesian coordinates using the (4.4), the dot products become

$$\begin{aligned}Q(\hat{z})&=A\int d\Omega'\,I(\hat{n}')\left(\cos^2\theta'\cos^2\phi'+\sin^2\phi'-\cos^2\theta'\sin^2\phi'-\cos^2\phi'\right)\\&=-A\int d\Omega'\,I(\hat{n}')\sin^2\theta'\cos 2\phi'\,.\end{aligned} \tag{4.39}$$

Now is crucial to recognise this combination of sines and cosines as being proportional to the sum of the spherical harmonics

$$Y_{2,2}+Y_{2,-2}=-\sqrt{\frac{15}{32\pi}}\left(\sin^2\theta e^{+2i\phi}+\sin^2\theta e^{-2i\phi}\right)=-\sqrt{\frac{15}{32\pi}}\left(\sin^2\theta\cos 2\phi)\right). \tag{4.40}$$

We can then expand the incident radiation field in spherical harmonics

$$I'(\theta',\phi')=\sum_{l=0}^{\infty}\sum_{m=-l}^{l}a_{lm}Y_{lm}(\theta',\phi')\,. \tag{4.41}$$

Since the spherical harmonics are orthogonal, the integral will select only the $l=2$, $m=\pm 2$ components of the distribution I. Because of this, nonzero Q will be produced only if the incident radiation has a quadrupole moment.

The same derivation could be done, mutatis mutandis, for the U component ($\hat{x}$ and $\hat{y}$ must be replaced by unit vectors rotated $\pi/4$, i.e $(\hat{x}+\hat{y})/2$ and $(\hat{x}-\hat{y})/2$), one will find

$$U(\hat{z})=-A\int d\Omega'\,I(\hat{n}')\sin^2\theta'\sin 2\phi'\,. \tag{4.42}$$

where the sines are proportional to $Y_{2,2}-Y_{2,-2}$. Again, an incident quadrupole is needed.

Remembering the definition (4.32) we can write

$$Q(\hat{z}) + iU(\hat{z}) \propto Y_{2,2}(\hat{n}')\,; \qquad Q(\hat{z}) - iU(\hat{z}) \propto Y_{2,-2}(\hat{n}') \tag{4.43}$$

and so

$$Q(\hat{z}) \propto \Re(a_{22})\,; \qquad U(\hat{z}) \propto \Im(a_{22})\,. \tag{4.44}$$

Thus polarization is generated along the outgoing z-axis provided that the a_{22} quadrupole moment of the incoming radiation is non-zero.

4.4.1 Arbitrary Scattering Direction

If we want to compute the outgoing polarization in a direction making an angle β with the $\hat{z}$-axis, the incoming radiation must be expanded in a coordinate system rotated through the Euler angle β. The rotated multipole coefficient are

$$\tilde{a}_{lm} = \int d\Omega\, Y^*_{lm}(R\Omega) I'(\Omega) = \sum_{m'=-m}^{m} D^{l\,*}_{m'm}(R) \int d\Omega\, Y^*_{lm'}(\Omega) I'(\Omega)\,; \tag{4.45}$$

where R is the rotation operator and $D^l_{m'm}$ is the Wigner D-symbol. In this new frame we can thus use the previous result where, instead of a_{22}, the multipole coefficient generating polarization will be $\tilde{a}_{22}$.

If the incoming radiation has an azimuthal simmetry, in other words is independent of ϕ, then the only non-zero component of the multipole is

$$\tilde{a}_{22} = a_{20} d^{2\,*}_{02}(\beta) = \frac{\sqrt{6}}{4} a_{20} \sin^2\beta\,. \tag{4.46}$$

And the related Stokes parameter will be

$$Q(\hat{n}) + iU(\hat{n}) \propto a_{20} \sin^2\beta\,; \tag{4.47}$$

but since the incoming field is real, a_{20} will be real, and so it must be $U = 0$.

An azimuthally-symmetric radiation field will thus generate a pure Q scattered field, which means that the polarization orientation will be in the plane of the $\hat{z}$-axis and the scattering direction and its magnitude will be proportional to $\sin^2\beta$.

4.4.2 Scattering From an Electron Cloud

Up to now we have considered the polarization emerging in a certain direction from an incoming radiation field scattered by a single electron. But the reality of the CMB is way more complicated, there are lots of electrons coupled to the photon distribution. The formal approach to this type of

problems would request the use of the Boltzmann equation to describe the evolution of the various particles distributions in the phase space giving the interaction between them. We will not go down this path. In the following chapter we will show that the physics of the CMB polarization can be understood, at least in a intuitive way, by focusing on a single electron and a single plane wave mode of the density perturbation.

Chapter 5

CMB Polarization

In the previous Chapter we have seen how linear polarization can be generated by Thomson scattering if the incident field possesses a quadrupole anisotropy. Since electron-photon scattering stops at recombination, observing polarization in the CMB radiation means looking directly at the last scattering surface of the photons. For this reason detection and analysis of the polarization power spectrum provides an important tool for understanding the origin an the evolution of the early Universe. Besides providing more constrains for the estimations of cosmological parameters, the study of CMB polarization (in particular an eventual detection of a B-mode) in would be the smoking gun for the existence of primordial gravitational waves, thus giving an experimental proof for the theory of inflation. The degree of polarization depends on the duration of last scattering, according to the Standard Cosmological Model 10% of the anisotropies should be polarized. Since the temperature anisotropies are at the 10^{-5} level, the upper limit for the polarized signal is 10^{-6}, meaning μK. Although this represent a significant experimental challenge, the DASI experiment detected E polarization modes in 2002.

In this Chapter we will present an introduction to the polarization of the CMB, its origin and how quadrupole moments are generated. We will introduce the E-B decomposition of the polarization tensor and understand how these patterns are modulated over the last scattering surface. Finally, we will describe why B modes are related to primordial gravitational waves.

As we already said, the formal approach to this topic would request the use of the Boltzmann equation. Instead, we will focus on a single electron and a single plane wave modulation of the anisotropies, following a derivation that, even if it could appear too much intuitive and qualitative, let us understand quite well the physics behind the CMB polarization.

5.1 Local Quadrupoles

In terms of a decomposition of the incident radiation field into spherical harmonics $Y_l^2(\theta, \phi)$, the quadrupole is represented by $l = 2$, $m = 0, \pm 1, \pm 2$. This values of the index m correspond to scalar, vector and tensor perturbations in the temperature distribution, respectively. Since it could be shown that vector mode are supressed in the modulation, we will focus only on scalar and vector modes.

5.1.1 Scalar Modes

Let consider a single Fourier component of the temperature fluctuation, a single plane wave in the form $\exp(i\vec{k} \cdot \vec{x})$. The temperature and the gravitational potential gradients will cause a bulk flow of photons. We can group this two effect defining an effective temperature

$$(\Delta T/T)_{eff} = \Delta T/T + \Psi \,, \tag{5.1}$$

where Ψ is the gravitational potential, so the flows will always be from hot to cold effective temperature regions. Let consider an electron located in a trough of a plane wave, with reference to the figure (3.6) it will see a quadrupole anisotropy in the temperature pattern with azimuthal symmetry along $\vec{k}$, because hotter photons from the crest flow into the through from the $\pm\vec{k}$ directions while cold photons surround the electron in the plane. The pattern is a $m = 0$ quadrupole

$$Y_2^0 \propto 3\cos^2\theta - 1 \,, \tag{5.2}$$

where $\cos\theta = \hat{n} \cdot \hat{k}$.

If the electron is on a crest, the flow is the opposite direction. This means a reverse sign in the quadrupole but does not change the $m = 0$ nature. The full effect is thus described by a $m = 0$ quadrupole modulated by a plane wave

$$-Y_2^0 \exp(i\vec{k} \cdot \vec{x}) \,, \tag{5.3}$$

where the minus sign is because the photons flow from hot to cold regions.

In term of the Stokes parameters, the scalar pattern represent a pure Q field

$$Q = \sin^2\theta; \qquad U = 0 \,. \tag{5.4}$$

The reason of the sine can be understood remembering that the polarization peaks when the incident field varies in the direction orthogonal to the observation vector $\hat{n}$.

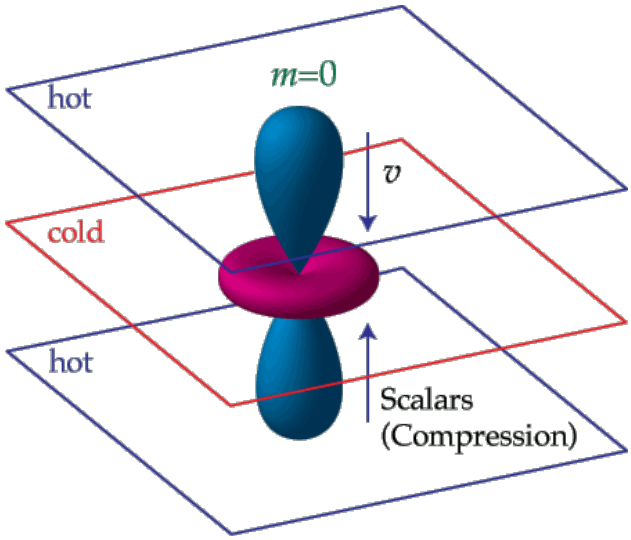

Figure 5.1: The scalar quadrupole moment $m = 0$. The bulk velocity $\vec{v}$ is perpendicular to the wave vector $\vec{k}$.

5.1.2 Tensor Modes

Tensor modes are generated by plane gravitational waves, transverse-traceless perturbation to the metric that distort a circle of test particles into an ellipse whose axes vary in time. This leds to a stretching of the wavelength of the photons, producing a $m = \pm 2$ pattern

$$Y_2^{\pm 2} \propto \sin^2\theta e^{\pm 2i\phi} \tag{5.5}$$

where (θ, ϕ) are polar coordinates defined along $\hat{k}$. Here the polarization is maxim at the pole and the Stokes parameters are

$$Q = (1 + \cos^2\theta)e^{2i\phi}; \qquad U = -2i\cos\theta e^{2i\phi}\,. \tag{5.6}$$

5.1.3 Superposition

Polarization patterns separate cleanly into $m = 0, \pm 1, \pm 2$ patterns for a single plane wave perturbation, where the coordinate system is defined by $\vec{k}$. But if we consider a superposition of various fluctuations with different $\vec{k}$, the polarization does not separe into $m = 0, \pm 1, \pm 2$ modes. On the contrary, because of statistical isotropy, the ensemble average power for each multipole l is independent of m. Nonetheless, the parity of the polarization patterns and its correlation with the temperature fluctuations survive the superposition. In the following section we will develop a formalism that will allow us to describe such a superposition.

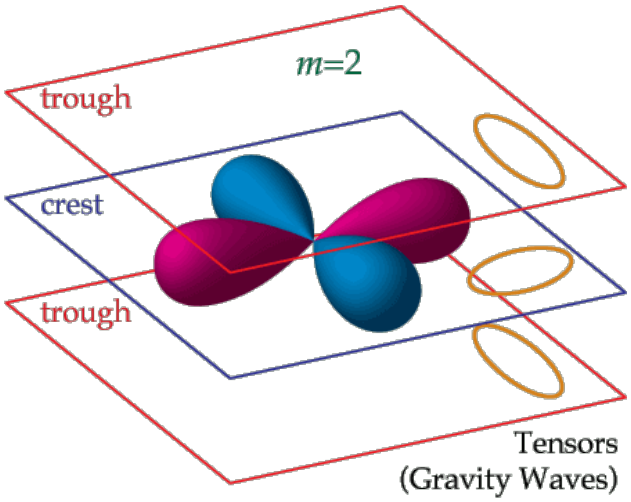

Figure 5.2: The tensor quadrupole moment $m = 2$. The circle of test particles is deformed by the passing gravitational wave, passing from crest to trough the major/minor axes are inverted.

5.2 E-B Decomposition

We have shown how the polarization can be quantified by the Stokes parameters $Q(\hat{n})$ and $U(\hat{n})$ measured as a function of position $\hat{n} = (\theta, \phi)$ in the sky. But they depend on the coordinate system that we choose, in this section we will thus develop a coordinate-system-indipendent representation of the tensor field P_{ab}.

5.2.1 Flat Sky

On a flat sky (which is a good approximation for a small region of sky) the polarization tensor as a function of the position $\vec{\theta} = (\theta_x, \theta_y)$ is

$$P_{ab} = \frac{1}{2} \begin{pmatrix} Q(\vec{\theta}) & U(\vec{\theta}) \\ U(\vec{\theta}) & -Q(\vec{\theta}) \end{pmatrix} . \tag{5.7}$$

We now define gradient 'E' and curl 'B' components of the tensor field as follows:

$$\nabla^2 P_E = \partial_a \partial_b P_{ab} \tag{5.8}$$
$$\nabla^2 P_G = \epsilon_{ac} \partial_b \partial_c P_{ab} \tag{5.9}$$

where ϵ_{ac} is the two dimensional Levi-Civita tensor.

If we write the Fourier transform for P_{ab}

$$P_{ab}(\vec{\theta}) = \int \frac{d^2\vec{l}}{(2\pi)^2} \tilde{P}_{ab}(\vec{l}) e^{-i\vec{l}\cdot\vec{\theta}} \tag{5.10}$$

$$\tilde{P}_{ab}(\vec{l}) = \int d^2\vec{\theta} \tilde{P}_{ab}(\vec{\theta}) e^{i\vec{l}\cdot\vec{\theta}} \tag{5.11}$$

the right member of equations (5.8) becomes

$$\partial_a\partial_b P_{ab}(\vec{\theta}) = \partial_a\partial_b \int \frac{d^2\vec{l}}{(2\pi)^2} \tilde{P}_{ab}(\vec{l}) e^{-i\vec{l}\cdot\vec{\theta}} = \int \frac{d^2\vec{l}}{(2\pi)^2} \tilde{P}_{ab}(\vec{l}) \partial_a\partial_b e^{-i\vec{l}\cdot\vec{\theta}} =$$
$$= \frac{1}{2} \int \frac{d^2\vec{l}}{(2\pi)^2} \left[\tilde{Q}(\vec{l}) l_x^2 + 2 l_x l_y \tilde{U}(\vec{l}) - \tilde{Q}(\vec{l}) l_y^2 \right] e^{-i\vec{l}\cdot\vec{\theta}} \tag{5.12}$$

where in the last passage we have written the explicit components of (5.7).

But the left member of (5.8) is simply the operator ∇^2 applied to the (5.10)

$$\nabla^2 P_E(\vec{\theta}) = \int \frac{d^2\vec{l}}{(2\pi)^2} (l_x^2 + l_y^2) \tilde{P}_{ab}(\vec{l}) e^{-i\vec{l}\cdot\vec{\theta}} . \tag{5.13}$$

Imposing equality between (5.12) and (5.13) we find an expression for $\tilde{P}_E(\vec{l})$. The same calculations can be done for $\tilde{P}_E(\vec{l})$. We have thus demonstrate that the Fourier components of $P_E(\vec{\theta})$ and $P_G(\vec{\theta})$ are

$$\tilde{P}_E(\vec{l}) = \frac{1}{2} \frac{(l_x^2 - l_y^2)\tilde{Q}(\vec{l}) + 2 l_x l_y \tilde{U}(\vec{l})}{l_x^2 + l_y^2} \tag{5.14}$$

$$\tilde{P}_G(\vec{l}) = \frac{1}{2} \frac{2 l_x l_y \tilde{Q}(\vec{l}) - (l_x^2 - l_y^2)\tilde{U}(\vec{l}))}{l_x^2 + l_y^2} . \tag{5.15}$$

Invariance Under Rotations

We want to verify that the Fourier components $\tilde{P}_E$ and $\tilde{P}_B$ are invariant under a rotation of the $\theta_x - \theta_y$ axes.

In the previous chapter we have shown how objects transform under a rotation $R(\alpha)$, recalling equation (4.27) and (4.28)

$$\begin{pmatrix} l'_x \\ l'_y \end{pmatrix} = \begin{pmatrix} \cos\alpha & \sin\alpha \\ -\sin\alpha & \cos\alpha \end{pmatrix} \begin{pmatrix} l_x \\ l_y \end{pmatrix} \tag{5.16}$$

$$\begin{pmatrix} Q' \\ U' \end{pmatrix} = \begin{pmatrix} \cos 2\alpha & \sin 2\alpha \\ -\sin 2\alpha & \cos 2\alpha \end{pmatrix} \begin{pmatrix} Q \\ U \end{pmatrix} . \tag{5.17}$$

Rotation invariance for $\tilde{P}_E$ is proved if

$$\tilde{P}'_E(\vec{l}') = \frac{1}{2} \frac{(l_x^{2\prime} - l_y^{2\prime})\tilde{Q}'(\vec{l}') + 2 l'_x l'_y \tilde{U}'(\vec{l})}{l_x^{2\prime} + l_y^{2\prime}} = \tilde{P}_E(\vec{l}) . \tag{5.18}$$

Note that $l_x^{2\prime} + l_y^{2\prime}$ is manifestly invariant, we will then focus only on the numerator.

$$\begin{aligned}(l_x^{2\prime} - l_y^{2\prime}) &= (l_x \cos\alpha + l_y \sin\alpha)^2 - (-l_x \sin\alpha + l_y \cos\alpha)^2 \\ &= l_x^2 \cos^2\alpha + l_y^2 \sin^2\alpha + 2l_x l_y \cos\alpha \sin\alpha - l_x^2 \sin^2\alpha - l_y^2 \cos^2\alpha + 2l_x l_y \cos\alpha \sin\alpha \\ &= (l_x^2 - l_y^2)(\cos^2\alpha - \sin^2\alpha) + 4l_x l_y \cos\alpha \sin\alpha \\ &= (l_x^2 - l_y^2)(\cos 2\alpha) + 2l_x l_y \sin 2\alpha \end{aligned} \tag{5.19}$$

$$\begin{aligned}(l_x' l_y') &= (l_x \cos\alpha + l_y \sin\alpha)(-l_x \sin\alpha + l_y \cos\alpha) \\ &= -l_x^2 \cos\alpha \sin\alpha + l_x l_y \cos^2\alpha - l_x l_y \sin^2\alpha + l_y^2 \cos\alpha \sin\alpha \\ &= (l_x l_y)(\cos^2\alpha \sin^2\alpha) - (l_x^2 - l_y^2)\cos\alpha \sin\alpha \\ &= l_x l_y \cos 2\alpha - \frac{(l_x^2 - l_y^2)}{2} \sin 2\alpha \,. \end{aligned} \tag{5.20}$$

And so, substituting in the numerator

$$\begin{aligned}&[(l_x^2 - l_y^2)(\cos 2\alpha) + 2l_x l_y \sin 2\alpha](\tilde{Q} \cos 2\alpha + \tilde{U} \sin 2\alpha) + \\ &+ [2l_x l_y \cos 2\alpha - (l_x^2 - l_y^2)\sin 2\alpha](-\tilde{Q} \sin 2\alpha + \tilde{U} \sin 2\alpha) = \\ &= (l_x^2 - l_y^2)\tilde{Q} \cos^2 2\alpha + 2l_x l_y \tilde{Q} \sin 2\alpha \cos 2\alpha + (l_x^2 - l_y^2)\tilde{U} \cos 2\alpha \sin 2\alpha + 2l_x l_y \tilde{U} \sin^2 2\alpha + \\ &- 2l_x l_y \tilde{Q} \sin 2\alpha \cos 2\alpha + (l_x^2 - l_y^2)\tilde{Q} \sin^2 2\alpha + 2l_x l_y \tilde{U} \cos^2 2\alpha - (l_x^2 - l_y^2)\tilde{U} \cos 2\alpha \sin 2\alpha = \\ &= (l_x^2 - l_y^2)\tilde{Q}(\vec{l}) + 2l_x l_y \tilde{U}(\vec{l}) \,. \end{aligned} \tag{5.21}$$

That proves the invariance. The calculations for $\tilde{P}_G$ are exactly the same.

5.2.2 Power Spectra and Parity

As we saw in Chaper 3 the temperature power spectrum C_l^{TT} is defined from

$$\langle \tilde{T}(\vec{l}) \tilde{T}(\vec{l}') = (2\pi)^2 \delta(\vec{l} + \vec{l}') C_l^{TT} \,. \tag{5.22}$$

Likewise, we can define the polarization power spectra as

$$\langle \tilde{P}_E(\vec{l}) \tilde{P}_E(\vec{l}') = (2\pi)^2 \delta(\vec{l} + \vec{l}') C_l^{EE} \tag{5.23}$$

$$\langle \tilde{P}_B(\vec{l}) \tilde{P}_B(\vec{l}') = (2\pi)^2 \delta(\vec{l} + \vec{l}') C_l^{BB} \tag{5.24}$$

$$\langle \tilde{P}_E(\vec{l}) \tilde{P}_B(\vec{l}') = (2\pi)^2 \delta(\vec{l} + \vec{l}') C_l^{EB} \,. \tag{5.25}$$

If we also consider cross-correlation of the polarization with temperature, then we have six power spectra

$$\langle \tilde{X}_1(\vec{l}) \tilde{X}_2(\vec{l}') = (2\pi)^2 \delta(\vec{l} + \vec{l}') C_l^{X_1 X_2} \tag{5.26}$$

where $X_1, X_2 = \{T, P_E, P_B\}$

Now consider a parity inversion, for example a reflection about the x-axis. Then we have

$$\theta_y \to -\theta_y; \qquad Q \to Q; \qquad U \to -U; \qquad l_x \to l_x; \qquad l_y \to -l_y \tag{5.27}$$

and also

$$\tilde{T}(\vec{l}) \to \tilde{T}(\vec{l}); \qquad \tilde{P}_E(\vec{l}) \to \tilde{P}_E(\vec{l}); \qquad \tilde{P}_B(\vec{l}) \to \tilde{P}_B(\vec{l})\,. \tag{5.28}$$

This means that E and T are parity even, while B is parity odd. Thus, if the physics that gives rise to the fluctuations conserves parity we will have that

$$C_l^{TB} = C_l^{EB} \equiv 0 \forall l\,. \tag{5.29}$$

So the statistic of the T/P map is entirely determined by the four power spectra C_l^{TT}, C_l^{TE}, C_l^{EE} and C_l^{BB}.

5.2.3 Full Sky

The result we obtained in the previous section are valid only if we consider a small region of the sky, for bigger areas we need to account for the curvature of the celestial sphere. Thus, we will now develop the E-B formalism on the 2-sphere.

Using spherical polar coordinates (θ, ϕ) the 2-sphere has a metric

$$g_{ab} = \begin{pmatrix} 1 & 0 \\ 0 & \sin^2\theta \end{pmatrix}\,. \tag{5.30}$$

The polarization tensor is defined on the tangent plane to photon propagation and it must be symmetric $P_{ab} = P_{ba}$ and trace-free $g^{ab}P_{ab} = 0$, hence

$$P_{ab}(\hat{n}) = \frac{1}{2}\begin{pmatrix} Q(\hat{n}) & -U(\hat{n})\sin\theta \\ -U(\hat{n})\sin\theta & -Q(\hat{n})\sin^2\theta \end{pmatrix}\,. \tag{5.31}$$

If we denote with ':' the covariant derivative ∇_a and with ',' the ordinary one ∂_a, we can write the covariant derivatives of scalar, vector and tensor fields as

$$S_{:a} = S_{,a} \tag{5.32}$$
$$V^a_{:b} = V^a_{,b} + V^c\Gamma^a_{bc} \tag{5.33}$$
$$T^{ab}_{:c} = T^{ab}_{,c} + T^{db}\Gamma^a_{cd} + T^{ad}\Gamma^b_{cd} \tag{5.34}$$

where the Christoffel symbols are

$$\Gamma^a_{bc} = \frac{1}{2}g^{ad}(g_{db,c} + g_{dc,b} - g_{bc,d})\,. \tag{5.35}$$

It can be proved that any STF 2×2 tensor can be written as the 'gradient' of some scalar field $A(\hat{n})$ plus the 'curl' of some other scalar field $B(\hat{n})$

$$P_{ab} = [A_{:ab} - \frac{1}{2} g_{ab} A^{:c}_{c}] + \frac{1}{2}[B_{:ac}\epsilon^{c}_{b} + B_{:bc}\epsilon^{c}_{a}] \tag{5.36}$$

where the antisymmetric tensor is defined as

$$\epsilon_{ab} = \sqrt{g} \begin{pmatrix} 0 & 1 \\ -1 & 0 \end{pmatrix} . \tag{5.37}$$

Since any scalar field in the sphere can be expanded in spherical harmonics, it follows that the polarization tensor can be expanded in terms of gradients and curls of spherical harmonics

$$\frac{P_{ab}(\hat{n})}{T_0} = \sum_{l=2}^{\infty} \sum_{m=-l}^{l} \left[a^{E}_{(lm)} Y^{E}_{(lm)ab}(\hat{n}) + a^{B}_{(lm)} Y^{B}_{(lm)ab}(\hat{n}) \right] . \tag{5.38}$$

The expansion coefficients are given by

$$a^{J}_{lm} = \frac{1}{T_0} \int d\hat{n} P_{ab}(\hat{n}) Y^{J\,ab\,*}_{lm}(\hat{n}) \qquad \text{with } J = \{E, B\} \tag{5.39}$$

and

$$Y^{E}_{(lm)ab} = N_l \left(Y_{(lm):ab} - \frac{1}{2} g_{ab} Y^{c}_{(lm):c} \right) \tag{5.40}$$

$$Y^{B}_{(lm)ab} = \frac{N_l}{2} \left(Y_{(lm):ac}\epsilon^{c}_{b} + Y_{(lm):bc}\epsilon^{e}_{a} \right) \tag{5.41}$$

where the normalization factor N_l is

$$N_l = \sqrt{\frac{2(l-2)!}{(l+2)!}} . \tag{5.42}$$

Note that the reality of T, Q and U implies

$$a^{X\,*}_{(lm)} = (-1)^m a^{X}_{(l,-m)} \qquad \text{where } X = \{T, E, B\} . \tag{5.43}$$

The T/P power spectra are now

$$\langle a^{X\,*}_{(lm)} a^{X'}_{(l'm')} \rangle = C^{XX'}_{l} \delta_{ll'} \delta_{mm'} \qquad \text{for } X, X' = \{T, E, B\} . \tag{5.44}$$

As in the flat sky approximation, TB and EB are zero if parity is conserved.

5.2.4 Rotations

Note that if we rotate the polarization tensor P_{ab} by 45°, which means $(Q, U) \to (U, -Q)$, then $E \to B$ and $B \to -E$.

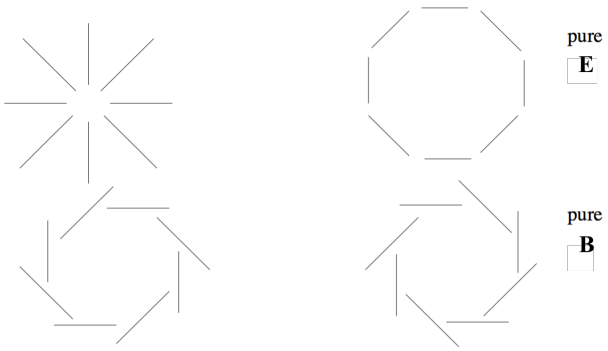

Figure 5.3: Examples of E (top) and B (bottom) polarization patterns. Clearly E modes are invariant under parity, while B modes are odd

5.3 Modulation Over the Last Scattering Surface

Because the spherical harmonics that describe the temperature anisotropy have $(-1)^l$ electric parity, Thomson scattering can only produce E-modes locally. Until now we have described the polarization patterns generated by a single electron on the last scattering surface, but the pattern we see in the sky is the modulation of all the local modes by the plane wave spatial dependence of the perturbation.

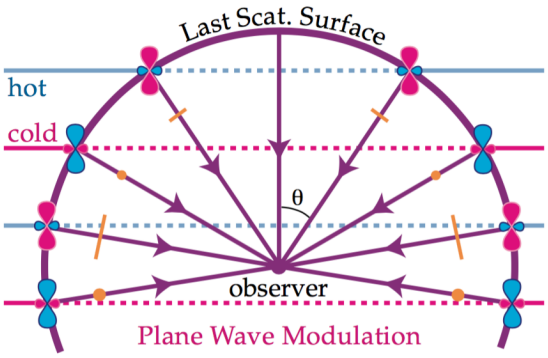

Figure 5.4: Modulation of a scalar local patter on the last scattering surface.

This modulations changes the amplitude and sign of the polarization but does not mix Q and U patterns. However, if the local pattern possesses a Q component, a B mode can be generated in the superposition. The reason why this occur can be understood by analyzing the local distinction between E and B modes. The definition (5.8) and (5.9) of these modes inolves the second derivatives of the polarization tensor and it could be shown that the Hessian of the polarization amplitude has principle axes on

the same sense as the polarization for E and 45° crossed with it for B. In a less mathematical way, it means that near a maximum of the polarization direction of change in the polarization is parallel/perpendicular and at 45° degree for E and B modes, respectively. But the plane wave modulation changes the polarization in the direction $\hat{k}$ (N-S) of the sphere, so a local Q pattern is needed to obtain a global B mode.

This superposition can be formally described and quantified by describing the plane wave modulation as the addition of an angular momentum Y_l^0 from the plane wave. This takes the $l = 2$ local angular dependence to higher l and splits the signals into E and B modes with ratios related to the Clebsch-Gordan coefficients.

What matters to us is the fact that, for scalars, the modulation is a pure Q-field and thus its E-mode nature is preserved. Local tensors patterns on the other hand are composed by both Q and U, which imply a nearly equal amount of E and B modes in the total pattern.

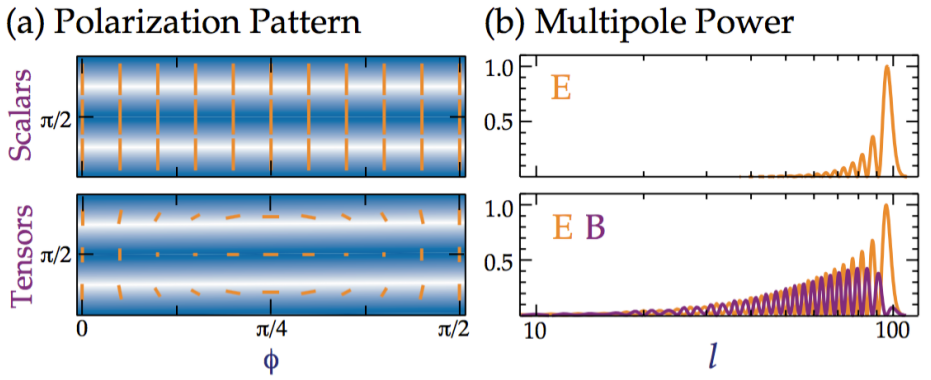

Figure 5.5: Modulation of locals scalar and tensor E-modes (a) by a single plane wave and the resulting predicted power spectrum (b).

A future detection of B modes in the CMB polarization pattern will thus be clear indication of the existance of primordial gravitational waves, leading to a strong experimental proof for the theory of inflation and an estimate of its energy scale.

5.4 Experimental Data

At the present time there are no accurate measurements of B-modes polarization, the 2014 data from the BICEP2 experiment were thought to be a clear sign of these modes but, later in the same year, it was understood that these result can be fully attributed to cosmic dust.

On the other hand, EE and TE power spectra are experimentally known since 2002, the following data are from the 2015 *Plank*'s data release.

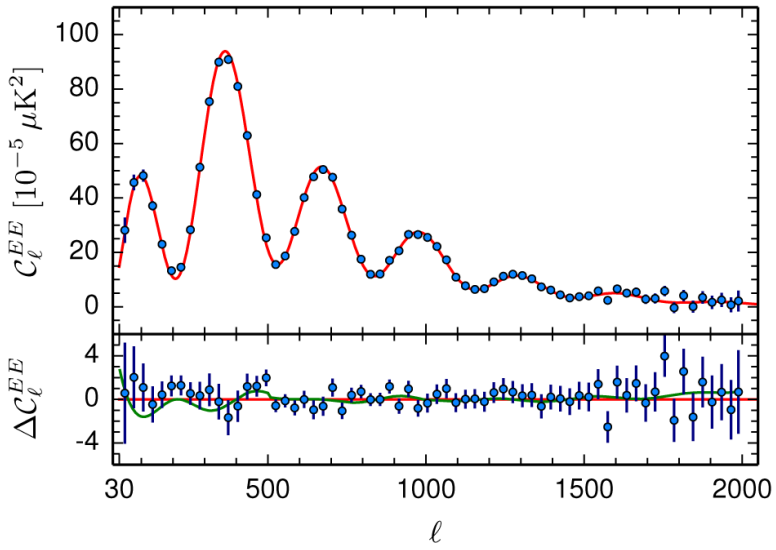

Figure 5.6: Planck 2015 EE power spectrum. The red line is the Planck best-fit primordial power spectrum. Residuals with respect to this model are shown in the lower panel. The error bars show $\pm 1\sigma$ uncertainties.

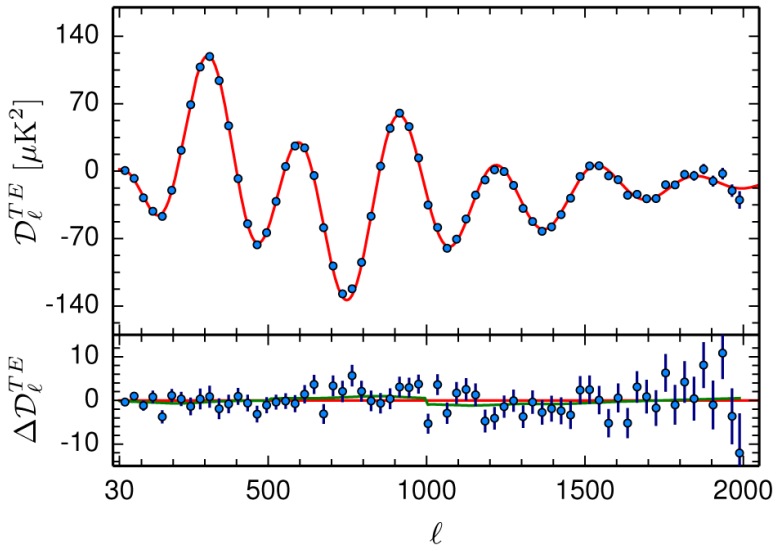

Figure 5.7: Planck 2015 TE power spectrum. The red line is the Planck best-fit primordial power spectrum. Residuals with respect to this model are shown in the lower panel. The error bars show $\pm 1\sigma$ uncertainties.

Bibliography

[1] P. Cabella and P. Kamionkowski, *Theory of Cosmic Microwave Background Polarization*, arXiv:astro-ph/0403392 (2004).

[2] P. Coles and F. Lucchin, *Cosmology - The Origin and Evolution of Cosmic Structure*, (John Wiley & Sons, 2002).

[3] S. Dodelson, *Modern Cosmology*, (Academic Press, 2003).

[4] W. Hu and S. Dodelson, *Cosmic Microwave Background Anisotropies*, arXiv:astro-ph/0110414 (2001).

[5] W. Hu and M. White, *A CMB Polarization Primer*, arXiv:astro-ph/9706147 (1997).

[6] A. Kosowsky, *Introduction to Microwave Background Polarization*, arXiv:astro-ph/9904102 (1999).

[7] K. Lechner, *Elettrodinamica Classica*, (Springer, 2014).

[8] A. Liddle, *An Introduction to Modern Cosmology*, (John Wiley & Sons, 2003).

[9] F. Lucchin, *Introduzione alla cosmologia*, (Zanichelli, 2003).

[10] Planck Collaboration, *Planck 2015 results. XIII. Cosmological parameters*, arXiv:1502.01589 (2015).

[11] G. B. Rybicki and A. P. Lightman, *Radiative Processes in Astrophysics*, (John Wiley & Sons, 1979).

[12] W. Hu's Tutorials: http://background.uchicago.edu/index.html.